Geomechanics and Engineering, *Vol. 13, No. 4 (2017) 685-699*
DOI: https://doi.org/10.12989/gae.2017.13.4.685

Pressure analysis in grouting and water pressure test to achieving optimal pressure

Hassan Bakhshandeh Amnieh[*1], Majid Masoudi[2a] and Reza Kolahchi[3b]

[1]*School of Mining, College of Engineering, University of Tehran, Iran*
[2]*Department of Mining Engineering, Faculty of Engineering, University of Kashan, Iran*
[3]*Department of Civil Engineering, Meymeh Branch, Islamic Azad University, Meymeh, Iran*

(*Received November 30, 2016, Revised April 2, 2017, Accepted April 27, 2017*)

Abstract. In order to determine the rate of penetrability, water pressure test is used before the grouting. One of the parameters which have the highest effect is pressure. Mathematical modeling is used for the first time in this study to determine the optimum pressure. Thus, the joints that exist in the rock mass are simulated using cylindrical shell model. The joint surroundings are also modeled through Pasternak environment. In order to validate the modeling, pressure values obtained by the model were used in the sites of Seymareh and Aghbolagh dams and the relative error rates were measured considering the differences between calculated and actual pressures recorded in these operations. In water pressure test, in Seymareh dam, the error values were equal to 4.75, 3.93, 4.8 percent and in the Aghbolagh dam, were 22.43, 5.22, 2.6 percent and in grouting operation in Seymareh dam were equal to 9.09, 32.50, 21.98, 5.57, 29.61 percent and in the Aghbolagh dam were 2.96, 5.40, 4.32 percent. Due to differences in rheological properties of water and grout and based on the overall results, modeling in water pressure test is more accurate than grouting and this error in water pressure test is 7.28 percent and in grouting is 13.92 percent.

Keywords: water pressure test; grouting; hydraulic fracture; mathematical modeling; cylindrical shell model

1. Introduction

Generally, grouting operation, is one of the ways to reduce water leakage, increase strength and consolidate jointed rock on the sites (Economides 1990). To determine the permeability of jointed rocks, in situ test that is called water pressure test (WPT) is usually used (Wong and Farmer 1993). In this test, water is penetrated at a certain section of the borehole under a variable pressure. Lugeon conducted the first water pressure test in 1933. The results of his tests have been the most common and best means of hydraulic evaluation for grouting in rock masses till now (Rice 1998). Despite its shortcomings, this test is one of the few methods that contain all the scientific and engineering aspects mentioned before.

Absorption of one liter of water per minute for each meter of the borehole at the pressure of one mega Pascal is equal to one lugeon: $1LU=1lit.min^{-1}.m^{-1}$ (Van Dam 1999).

∗Corresponding author, Associate Professor, E-mail: hbakhshandeh@ut.ac.ir
[a]Ph.D. Student, E-mail: Masoudi@Staff.kashanu.ac.ir
[b]Ph.D., E-mail: r.kolahchi@gmail.com

Copyright © 2017 Techno-Press, Ltd.
 ISSN: 2005-307X (Print), 2092-6219 (Online)

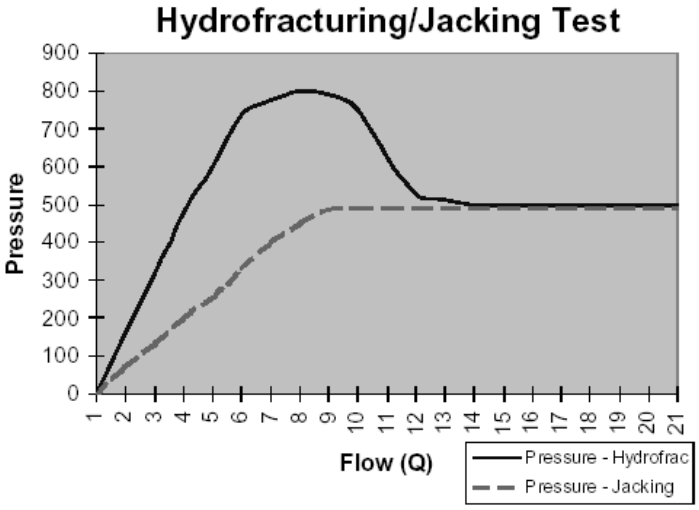

Fig. 1 The relationship between pressure and flow in hydro fracturing and jacking test (Tolppanen 2003)

Lugeon number is always between one and 100 and if this value is higher than 100, it is considered to be 100

$$LU=10Q/P_e \quad (1)$$

Where Q is the quantity of the water absorbed in liters per meter per minute, P_e is the highest effective pressure in the test and LU is the lugeon value. After doing water pressure test and determining the amount of water take, the sections that in terms of quality is poor and need for improvement is determined and in the following, by grouting can be sealing and consolidation.

One of the most important issues that must be investigated and prevented in the water pressure test and grouting is known as hydraulic fracturing (Garagash 2003). As can be seen in Fig. 1, when hydraulic fracturing happens, high pressure causes the rock mass to break. The dilation phenomenon through which the fractures present in the rock, open due to high pressure is sometimes called hydraulic jacking, too (Van de Ketterij 2001). However, it must be noted that conducting hydraulic fracture tests is absolutely essential to understand the fracturing behavior in the rock mass but such tests must be performed in a controlled manner since in most cases, the permeability of the waste caused by hydraulic fracturing is high (Wang 2009). In order to separate these two states, pressure and flow rates must be continuously recorded (Lhomme 2005). Fig. 1 shows the continuous recording of pressure and flow for hydro fracturing and jacking test (Tolppanen 2003).

Different types of stones, geological structures and in situ stress affect fracturing behavior and jacking in the rock mass. Therefore, the maximum pressure of the test will be also influenced by these factors (El Tani 2012). The foundation of dams is damaged by fracturing and jacking. Thus, the maximum pressure must not cause fracturing and jacking in the rock mass.

However, pressure must not be so low that prevents us from observing mechanical weaknesses. Critical pressure has a wide range. In weak rocks, very low pressures (for example, 5 bar) (Yew and Weng 2014), can cause fracturing regardless of the depth. In strong rocks, a high pressure is required to fracture the rock even in shallow depth. Generally, critical pressure is independent of

depth (Wang 2009).

Water pressure test can determine the rate of permeability and the necessity of grouting and estimate the rate of sealing resulted from grouting. It must be noted that in some sites there are rocks in which the recorded water take is low but the grout take is high. The reason for this is the fracturing of the rock mass due to high pressure in grouting (Van de Ketterij 2001). Therefore, it can be seen that the hydraulic fracturing phenomenon can take place in both water pressure test and grouting operations and thus it is very important to investigate this phenomenon and try to prevent its occurrence (Wang 2009).

In this research mathematical modeling is used for the first time to determine the optimum pressure. Thus, the joints that exist in the rock mass are simulated using cylindrical shell model. The joint surroundings are also modeled through Pasternak environment. Elastic buckling of a thin cylindrical shell was studied by Karam *et al.* (1995), Agrawal and Sobel (1997) investigated the weight compressions of cylindrical shells with various stiffness under axial compression. Buckling of cylindrical shells with metal foam cores was presented by Hutchinson and He (2000), Elastic stability of cylindrical shell with an elastic core under axial compression was investigated by Ghorbanpour Arani *et al.* (2007) using energy method. Ye *et al.* (2011), however, investigated bucking of a thin-walled cylindrical shell with foam core under axial compression. Junger and Mass (1952) studied coupled vibrations of fluid-filled cylindrical shell based on shear shell theory and discussed the free vibration of orthotropic cylindrical shells filled partially or completely with an incompressible, non-viscous fluid. The static instability of a nano beam with geometrical imperfections imperfections embedded in elastic foundation was investigated by Mohammadi *et al.* (2014), Using semi-analytical finite strip method, the buckling behavior of laminated composite deep as well as thick shell of revolution under follower forces which remain normal to the shell was investigated by Khayat *et al.* (2016).

Stress analyses of different structures have been studied by many researchers. Mechanical and thermal stresses in a functionally graded hollow cylinder were investigated by Jabbari *et al.* (2002). Analysis of the thermal stress behavior of functionally graded hollow circular cylinders was presented by Liew *et al.* (2003). You *et al.* (2005) presented elastic analysis of internally pressurized thick-walled functionally graded spherical pressure vessels. Dai *et al.* (2006) studied exact solutions for functionally graded pressure vessels subjected to a uniform magnetic field. Ghorbanpour Arani *et al.* (2011) investigated the effect of material in-homogeneity on the electro-thermo-mechanical behaviors of functionally graded piezoelectric rotating shaft. Also, they (2011) studied electro-thermo-mechanical behaviors of functionally graded piezoelectric spheres using the analytical method and ANSYS software. Retrofit design of damaged pre-stressed concrete cylinder pipes was presented by Lee and Lee (2013). With respect to the developmental works on elastic analysis of the cylinders, it should be noted that none of the research mentioned above has considered composite structure and their specific characteristics. Singh and Darip (2007) analyzed nonlinear vibration of a composite skew plate using a four-nodded shear flexible quadrilateral high-precision plate bending element. Nonlinear free vibration analysis of laminated composite skew thin plates was reported by Malekzadeh (2003) using DQM. Electro-thermo-mechanical nonlinear vibration and instability of a fluid, conveying a smart composite micro tube made of polyvinylidene fluoride (PVDF), were investigated by Ghorbanpour Arani *et al.* (2015) based on the modified couple stress theory and Timoshenko beam model.

Temperature-dependent nonlinear dynamic stability of functionally graded CNT reinforced visco-plate was present by Kolahchi *et al.* (2016). Dynamic stability and parametric resonance response of a piezoelectric nanoplate, considering the viscoelastic property of system based on

Kelvin-Voigt model, were investigated by Kolahchi *et al.* (2016). A fast converging and fairly accurate nonlinear simulation method to assess the behavior of reinforced concrete columns subjected to static-oriented pushover force and axial loading (sections under biaxial-bending moment and axial loading) was proposed by Sadeghi (2016). Shear behavior of reinforced concrete was studied by Broujerdian and Kazemi (2016) based on recently developed constitutive laws for normal strength concrete and mild steel bars using the nonlinear finite element method. A numerical simulation of laboratory model tests was carried out by Tavakoli Mehrjardi *et al.* (2016) to develop an understanding of the behavior of pipes in a trench prepared with three-dimensional reinforced (namely ‘‘geocell-reinforced’’ in the present study) sand and rubber-soil mixtures, under repeated loadings. A nonlinear finite element algorithm was proposed by Sadeghi (2016) to analyze the reinforced concrete (RC) columns subjected to cyclic biaxial bending moment and axial loading

2. Mathematical modeling

A schematic diagram, of a cylindrical shell is shown in Fig. 2 in which geometrical parameters of length, L, radius, R and thickness h are also indicated. The surrounding foundation is simulated with spring and shear constants.

2.1 Stress-strain relations

Shear strains γxz, $\gamma \theta z$ are considered negligible in the Kirchhoff deformation theory. Hence, the tangential displacements u, v become linear function of the radial coordinate (z) (Arani *et al.* 2011). In other words

$$v(x,\theta,z) = v(x,\theta) - z\frac{\partial w(x,\theta)}{\partial \theta},$$
$$u(x,\theta,z) = u(x,\theta) - z\frac{\partial w(x,\theta)}{R\partial x}, \quad w(x,\theta,z) = w(x,\theta). \tag{2}$$

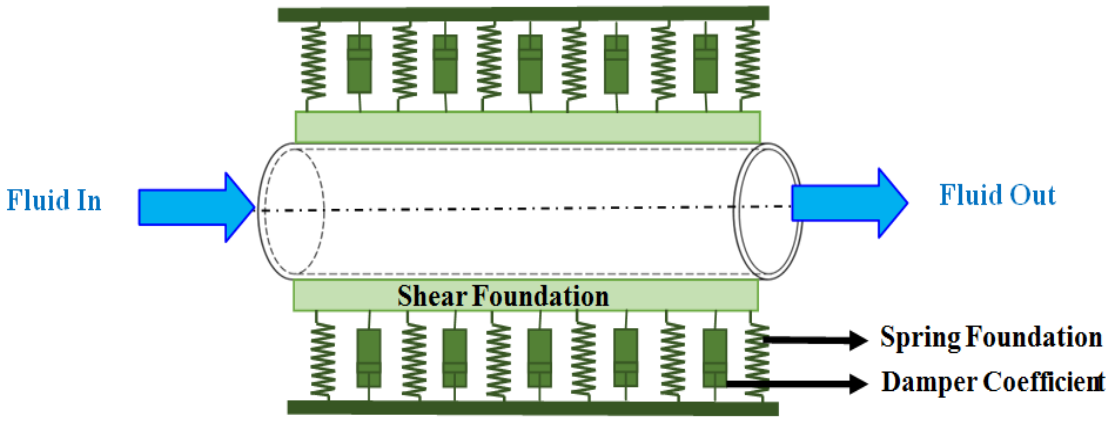

Fig. 2 A schematic figure of embedded cylindrical shell.

The strain components $\bar{\varepsilon}_{xx}$, $\bar{\varepsilon}_{\theta\theta}$ and $\bar{\gamma}_{x\theta}$ at an arbitrary point of the shell are related to the middle surface strains ε_{xx}, $\varepsilon_{\theta\theta}$ and $\gamma_{x\theta}$ and to the changes in the curvature and torsion of the middle surface k_{xx}, $k_{\theta\theta}$ and $k_{x\theta}$ by the following relationships

$$\begin{Bmatrix} \overline{\varepsilon_{xx}} \\ \overline{\varepsilon_{\theta\theta}} \\ 2\overline{\varepsilon_{x\theta}} \end{Bmatrix} = \begin{Bmatrix} \varepsilon_{xx} \\ \varepsilon_{\theta\theta} \\ \gamma_{x\theta} \end{Bmatrix} - z \begin{Bmatrix} k_{xx} \\ k_{\theta\theta} \\ k_{x\theta} \end{Bmatrix} = \left(\begin{bmatrix} \frac{\partial}{\partial x} & 0 & 0 \\ 0 & \frac{\partial}{R\partial\theta} & \frac{1}{R} \\ \frac{\partial}{2R\partial\theta} & \frac{\partial}{2\partial x} & 0 \end{bmatrix} - z \begin{bmatrix} 0 & 0 & \frac{\partial^2}{\partial x^2} \\ 0 & 0 & \frac{\partial^2}{R^2\partial\theta^2} \\ 0 & 0 & 2\frac{\partial^2 w}{R\partial x\partial\theta} \end{bmatrix} \right) \times \begin{bmatrix} u \\ v \\ w \end{bmatrix}, \tag{3}$$

Where u, v and w, describe the displacements in the orthogonal coordinate system x, θ, z established at the middle surface of the shell.

Using Hook law, the constitutive equation may expressed follows (Ghorbanpour Arani 2011)

$$\begin{Bmatrix} \sigma_{xx} \\ \sigma_{\theta\theta} \\ \sigma_{x\theta} \end{Bmatrix} = \begin{bmatrix} C_{11} & C_{12} & 0 \\ C_{12} & C_{22} & 0 \\ 0 & 0 & C_{66} \end{bmatrix} \left[\begin{Bmatrix} \frac{\partial u}{\partial x} \\ \frac{\partial v}{R\partial\theta} + \frac{w}{R} \\ \frac{\partial u}{R\partial\theta} + \frac{\partial v}{\partial x} \end{Bmatrix} - z \begin{Bmatrix} \frac{\partial^2 w}{\partial x^2} \\ \frac{\partial^2 w}{R^2\partial\theta^2} \\ 2\frac{\partial^2 w}{R\partial x\partial\theta} \end{Bmatrix} \right], \tag{4}$$

Where σ_{ij} (i,j=x,θ) stresses as well as u,v,w are the displacements of an arbitrary point of the shell in the axial, circumferential and radial directions, respectively. Also, C_{ij}, i,j=1,…6), correspond to elastic constants.

2.2 Energy method

The total potential energy of the pipe is the sum of strain energy, kinetic energy and work down by flowing fluid is expressed below where the strain energy is

$$\begin{aligned} U = \int_{-\frac{h}{2}}^{\frac{h}{2}} \iint_A \Bigg(& \sigma_{xx} \left(\frac{\partial u}{\partial x} - z\frac{\partial^2 w}{\partial x^2} \right) + \sigma_{\theta\theta} \left(\frac{\partial v}{R\partial\theta} + \frac{w}{R} + -z\frac{\partial^2 w}{R^2\,\partial\theta^2} \right) \\ & + \sigma_{x\theta} \left(\frac{\partial u}{R\partial\theta} + \frac{\partial v}{\partial x} - 2z\frac{\partial^2 w}{R\partial\theta\,\partial x} \right) \Bigg) dz\, dA, \end{aligned} \tag{5}$$

and the kinetic energy is

$$K = \frac{\rho}{2} \int_v \left((\frac{\partial u}{\partial t})^2 + (\frac{\partial v}{\partial t})^2 + (\frac{\partial w}{\partial t})^2 \right) dV, \tag{6}$$

and the work down by internal viscose fluid is (Wang and Ni 2009)

$$W=\int(F_{fluid})wdA=\int\Bigg(-h\rho_f\left(\frac{\partial^2 w}{\partial t^2}+2v_x\frac{\partial^2 w}{\partial x\partial t}+{v_x}^2\frac{\partial^2 w}{\partial x^2}\right)+h\mu\left(\frac{\partial^3 w}{\partial x^2\partial t}+\frac{\partial^3 w}{R^2\partial\theta^2\partial t}+v_x\left(\frac{\partial^3 w}{\partial x^3}+\frac{\partial^3 w}{R^2\partial\theta^2\partial x}\right)\right)\Bigg)wdA. \tag{7}$$

Now replacing these in the following expression based on the Hamilton principal

$$\int_0^t(\delta K-\delta U+\delta W)dt=0, \tag{8}$$

and defining the following non-dimensional quantities

$$\{\bar{u},\bar{v},\bar{w}\}=\frac{\{u,v,w\}}{h},\quad \gamma=\frac{h}{l},\quad \xi=\frac{x}{l},\quad \beta=\frac{h}{R},\ \bar{C}_{ij}=\frac{C_{ij}}{C_{11}},$$
$$\bar{\rho}=\frac{\rho_s}{\rho_f},\quad \mu=\frac{\mu_0}{h\sqrt{C_{11}\rho_f}},\quad V=v_x\sqrt{\frac{\rho_f}{C_{11}}},\quad \bar{t}=\frac{t}{h\sqrt{\frac{\rho_f}{C_{11}}}}, \tag{9}$$

The four electro-thermo mechanical coupling governing equations of PVDF cylindrical shell conveying viscose fluid, can therefore be written as

$$\gamma^2\left(\frac{\partial^2\bar{u}}{\partial\xi^2}+\frac{\partial\bar{w}}{\partial\xi}\frac{\partial^2\bar{w}}{\partial\xi^2}\right)+\gamma\beta\bar{C}_{12}\left(\frac{\partial^2\bar{v}}{\partial\xi\partial\theta}+\frac{\partial\bar{w}}{\partial\xi}+\beta_s\frac{\partial\bar{w}}{\partial\theta}\frac{\partial^2\bar{w}}{\partial\xi\partial\theta}\right)+\beta\bar{C}_{66}\left(\beta\frac{\partial^2\bar{u}}{\partial\theta^2}+\frac{\partial^2\bar{v}}{\partial\xi\partial\theta}+\beta\frac{\partial\bar{w}}{\partial\xi}\frac{\partial^2\bar{w}}{\partial\theta^2}+\frac{\partial\bar{w}}{\partial\xi}+\beta\frac{\partial\bar{w}}{\partial\theta}\frac{\partial^2\bar{w}}{\partial\xi\partial\theta}\right)+\gamma^2\bar{e}_{11}\frac{\partial^2\Phi}{\partial\xi^2}=(\bar{\rho})\frac{\partial^2\bar{u}}{\partial\bar{t}^2}, \tag{10}$$

$$\beta\bar{C}_{12}\left(\frac{\partial^2\bar{u}}{\partial\xi\partial\theta}+\frac{\partial\bar{w}}{\partial\xi}\frac{\partial^2\bar{w}}{\partial\xi\partial\theta}\right)+\beta^2\bar{C}_{22}\left(\frac{\partial^2\bar{v}}{\partial\theta^2}+\frac{\partial\bar{w}}{\partial\theta}+\beta\frac{\partial\bar{w}}{\partial\theta}\frac{\partial^2\bar{w}}{\partial\theta^2}\right)+\gamma\bar{C}_{66}\left(\beta\frac{\partial^2\bar{u}}{\partial\xi\partial\theta}+\frac{\partial^2\bar{v}}{\partial\xi^2}+\frac{\beta\partial^2\bar{w}}{\partial\theta\partial\xi}\frac{\partial\bar{w}}{\partial\xi}+\frac{\beta\partial\bar{w}}{\partial\theta}\frac{\partial^2\bar{w}}{\partial\xi^2}\right)+\beta\bar{e}_{12}\frac{\partial^2\Phi}{\partial\xi\partial\theta}=\bar{\rho}\frac{\partial^2\bar{v}}{\partial\bar{t}^2}, \tag{11}$$

$$\frac{\gamma^2}{12}\left(-\gamma^2\frac{\partial^4\bar{w}}{\partial\xi^4}-\bar{C}_{12}\beta^2\frac{\partial^4\bar{w}}{\partial\xi^2\partial\theta^2}\right)+\frac{1}{12}\left(-\gamma^2\beta^2\bar{C}_{12}\frac{\partial^4\bar{w}}{\partial\xi^2\partial\theta^2}-\beta^4\bar{C}_{22}\frac{\partial^4\bar{w}}{\partial\theta^4}\right)-\frac{\gamma\beta\bar{C}_{12}}{3}\left(\frac{\partial\bar{u}}{\partial\xi}+\frac{\gamma}{2}\left(\frac{\partial\bar{w}}{\partial\xi}\right)^2\right)-\beta\bar{C}_{22}\left(\frac{\partial\bar{v}}{\partial\theta}+\beta\bar{w}+\frac{\beta^2}{2}\left(\frac{\partial\bar{w}}{\partial\theta}\right)^2\right)-\left[\frac{\partial^2\bar{w}}{\partial\bar{t}^2}+2\gamma V\frac{\partial^2\bar{w}}{\partial\xi\partial\bar{t}}+\gamma^2V^2\frac{\partial^2\bar{w}}{\partial\xi^2}\right]-\mu\left[\gamma^2\frac{\partial^3\bar{w}}{\partial\xi^2\partial\bar{t}}+V\gamma^3\frac{\partial^3\bar{w}}{\partial\xi^3}+\beta^2\left(\frac{\partial^3\bar{w}}{\partial\theta^2\partial\bar{t}}+V\gamma\frac{\partial^3\bar{w}}{\partial\theta^2\partial\xi}\right)\right]+\gamma\beta\bar{e}_{12}\frac{\partial\Phi}{\partial\xi}=\bar{\rho}\frac{\partial^2\bar{w}}{\partial\bar{t}^2}, \tag{12}$$

2.3 Navier method

Considering simply supported boundary condition, the mechanical displacement may be written as

$$u(x,\theta) = u_0 \cos(\frac{n\pi x}{L}) \sin(m\theta), \tag{13}$$

$$v(x,\theta) = v_0 \sin(\frac{n\pi x}{L}) \cos(m\theta), \tag{14}$$

$$w(x,\theta) = w_0 \sin(\frac{n\pi x}{L}) \sin(m\theta), \tag{15}$$

Substituting Eq. (9) into Eqs. (6)-(8) results

$$\begin{bmatrix} K_{11} & K_{12} & K_{13} \\ K_{21} & K_{22} & K_{23} \\ K_{31} & K_{32} & K_{33} \\ \end{bmatrix} \begin{bmatrix} u_0 \\ v_0 \\ w_0 \end{bmatrix} = 0, \tag{16}$$

Solving the above equation, the displacement may be obtained. However, using the obtained displacement and Eq. (7), the pressure of fluid can be calculated.

3. Modeling details

In the mathematical model, the parameters shown in Table 1 were inserted into the modeling as the input data.

4. Case study

4.1 Seymareh dam

Table 1 A list of input data in modeling

Row	Name of the input parameter	Value of the input parameter
1	Dimensions of the given rock	1×1
2	Density of the rock	2.7 g/cm^3
3	Joint break (b)	1 mm
4	Elasticity module	1130 kg/m^3
5	Shear stiffness coefficient	10^9
6	Poisson coefficient	0.3
7	Grout penetration range	46.5 cm
8	Borehole radius	3.5 cm

Seymareh dam and its power plant are located in Iran, 40 km northwest of Dareshahr city and 7.5 km away from CheshmeShirin village in Ilam province. Its purpose is to use the potential power in Seymarehriver. Seymareh is a thin double-arched concrete dam with the height of 130 m from the present river bed (and about 180 m from the bedrock). Dam crest elevation is 730 m and at the normal elevation, water level is at the 720 m height above high sea level. The length of the dam crest at the elevated part of the dam crest is 202 m. The capacity of the dam reservoir is 3.215 billion cubic meters.

4.2 Aghbolagh dam

Aghbolagh earth dam is located at the distance of 32 km in the south of Borujen city in ChaharMahal-o-Bakhtiari province in Iran. The geographical coordinates of the dam axis in the UTM system are x=520363 and y=3512353. Considering the geological map, the area under study is located in the Zagros zone and under the Overthrust zone.

From the stratigraphic perspective, Mesozoic and Cenozoic rocks, especially the Cretaceous rocks are dominant in this zone and from the structural point of view, large faults such as the main Zagros fault and Dena fault play a major role in the zone.

5. Check the infiltrated fluid pressure values in water pressure test and grouting operations

In this section, the results achieved from water pressure test and grouting in boreholes of the Seymareh and Aghbolagh dams are shown in Tables 2 and 3. The resulting consists of pressure values in the some sections that hydraulic fracturing has occurred.

5.1 Estimation of hydraulic fracturing pressure in water pressure test using mathematical modeling

In this section, based on the results obtained in water pressure test from Seymareh and Aghbolagh dams and comparison of the real pressure values with the calculated pressure acquired through modeling, the results achieved by modeling were validated. In Table 4 comparison between these values and in Fig. 3, the amount of convergence among these is shown.

5.2 Estimation of hydraulic fracturing pressure in grouting using mathematical modeling

In this section, according to the real pressure values of obtained from grouting operation in Seymareh and Aghbolagh dams and comparison these with the calculated pressure acquired through modeling, the results achieved by modeling were validated. In Table 5 comparison between these values and in Fig. 4, the amount of convergence among these is shown. The resulting information consists of pressure values in the boreholes where water take in the water pressure test is low while grout take in the grouting operation is high. This shows that hydraulic fracturing has occurred in these sections. These data are shown in Table 5. In this section, cement grout pressure which led to the hydraulic fracturing in grouting is analyzed.

According to Table 2 in Seymareh dam, it can be seen that in the borehole P-19 in sections 3 and 4, in the borehole P-20 in section 6, in the borehole P-22 in section 4 and in the borehole P-23

Table 2 The results of water pressure test and grouting in boreholes of the Seymareh dam

Data obtained from P-22 borehole					Data obtained from P-20 borehole				
Number of section	Depth(m)	LU	P(pa)	V(m^3)	Number of section	Depth(m)	LU	P(pa)	V(m^3)
1	0-5	11.4	233000	0.021625	1	0-5	3.8	230000	0.012667
2	5-10	41.5	376000	0.032417	2	5-10	2.7	377000	0.012667
3	10-15	20.5	523000	0.068458	3	10-15	22.4	523000	0.0095
4	15-20	39.4	764000	7.291667	4	15-20	69.9	552000	5.216667
5	20-25	<1	964000	0.154208	5	20-25	<1	974000	0.015833
6	25-30	3.1	1162000	0.106833	6	25-30	22.8	1029000	7.654167
7	30-35	7	1299000	0.097375	7	30-35	1.34	1247000	0.025333
8	35-40	<1	1587000	0.005375	8	35-40	<1	1456000	0.022167
9	40-45	<1	1794000	0.010792	9	40-45	<1	1639000	0.019
10	45-50	6.4	2230000	0.022167	10	45-50	<1	2064000	0.015833
11	50-53	18.5	2082000	0.256125	11	50-53	19.54	1886000	2.6665
Data obtained from P-19 borehole					Data obtained from P-23 borehole				
Number of section	Depth(m)	LU	P(pa)	V(m^3)	Number of section	Depth(m)	LU	P(pa)	V(m^3)
1	0-5	54.3	130000	0.012667	1	0-5	51.3	225000	0.172625
2	5-10	29.8	377000	0.012667	2	5-10	72.2	343000	0.123333
3	10-15	10.9	521000	5.291667	3	10-15	10.3	522000	0.026667
4	15-20	6.7	695000	8.691667	4	15-20	5	767000	0.019458
5	20-25	11.54	1015000	0.006333	5	20-25	4.1	795000	0.049417
6	25-30	26.9	1066000	0.012667	6	25-30	95	1037000	3.110833
7	30-35	2.2	1291000	0.038	7	30-35	6.1	1207000	0.074667
8	35-40	4.5	1682000	0.022167	8	35-40	1.82	1445000	0.127667
9	40-45	<1	1743000	0.022167	9	40-45	<1	1663000	0.004833
10	45-50	3.6	3980000	0.019	10	45-50	3.8	2074000	0.021083
11	50-53	11.2	2381000	0.025325	11	50-53	18.2	2232000	3.98665

Table 3 Some results of the water pressure test and grouting in boreholes of the Aghbolagh dam

TG-1 Borehole				
The depth of boreholes(m)	RQD	LU	Final pressure (kg/cm^2)	Real take (m^3)
4-6	20	100	5	311
6-10	61	100	5	30
10-15	67.8	14	7.5	350
15-20	83	25	10	1057
20-25	53.5	1	13	378
25-30	22	2	12	2380
30-35	51.8	2	12	2474

Table 3 Continued

The depth of boreholes(m)	RQD	LU	Final pressure (kg/cm^2)	Real take (m^3)
35-40	30	1	15	1589
40-45	94.5	26	20	5921
TG-2 Borehole				
4-7.3	58.8	100	5	756
7.3-12	50	12	9	812
12-17	93.5	49	14	243
17-22	94.6	100	13	3052
22-27	45.5	1	10	147
27-32	76.3	1	15	126
32-45	90	2	24	4471
TG-3 Borehole				
4.2-5.8	9	100	5	609
5.8-8.3	83	100	5	266
8.3-13	41.5	37	5	189
13-18	58.8	1	7.5	126
18-23	15.3	1	7	112

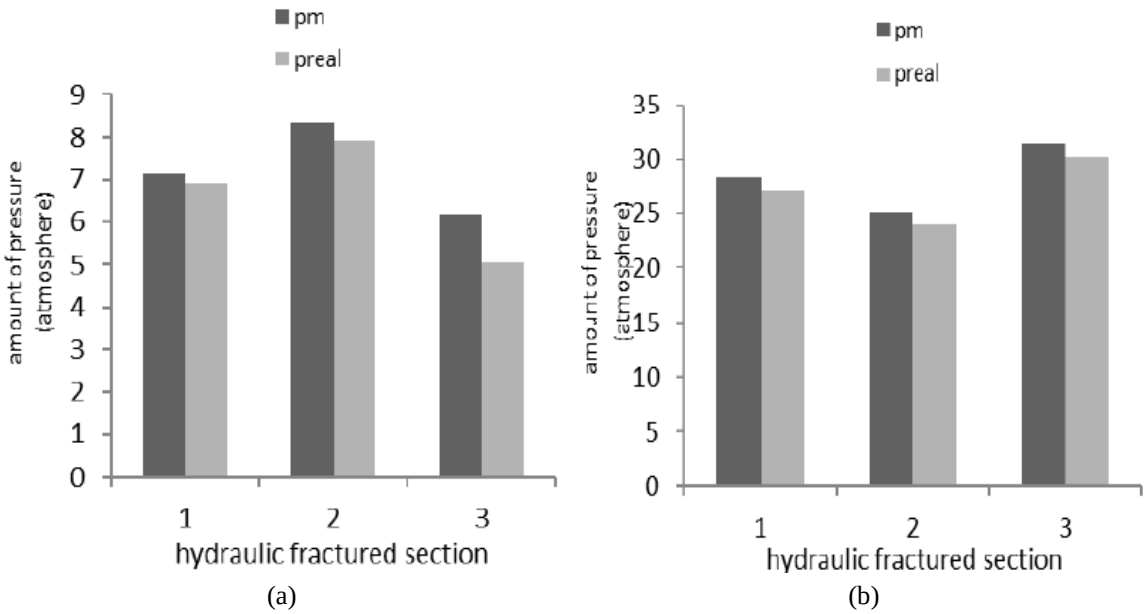

Fig. 3 Convergence rate between calculated fracturing pressure (P_m) and real fracturing pressure (P_{real}) in water pressure testin (a) Aghbolagh and (b) Seymareh dams

in section 11, the rate of water take obtained based on lugeon number is low while the cement grout take is high. Generally, this difference in the processes of water take and cement take

indicates the occurrence of hydraulic fracturing phenomenon due to excessive pressure in the grouting procedure.

In Aghbolagh dam, pilot grouting operation in the lime stones on the left side of the dam was carried out as the most important part of the whole grouting process with respect to sealing. The arrangement of TG-1, TG-2 and TG-3 grouting boreholes is in such a form that they are placed on the vertices of an equilateral triangle each side of which is as long as three meters. In each borehole, lugeon experiments are conducted first and after the acquisition of results, plans for the mixture of water, cement and other additives are selected. Grouting operation is carried out in five-meter-long sections and the results are shown in Table 3.

According to the results shown in Table 3, we can see that in the TG-1 borehole in the depths of 25-30 and 30-35 meters, the rate of water take is low (LU=2) while the amount of the grouted cement is high. The values of the variables just mentioned are 1175 and 1325, respectively. In the TG-2 borehole in the depth of 32-45 meters, the water take is also low (LU=2) but the cement take is very high and equals 2466 kg. The difference between low water absorption compared to high grout take indicates excessive increase in the grout's penetration pressure and occurrence of hydraulic fracturing in the grouting process.

Table 4 Comparison between water pressures that result in hydraulic fracturing in water pressure test and the calculated fracturing pressure in atmosphere

Seymareh dam		Aghbolagh dam	
Calculated pressure	Recorded pressure	Calculated pressure	Recorded pressure
28.421	27.13	7.121	6.94
25.174	24.02	8.323	7.91
31.387	30.2	6.195	5.06

Table 5 Comparison between grout pressures that result in hydraulic fracturing in grouting operations and the calculated fracturing pressure in atmosphere

Seymareh dam				Aghbolagh dam			
Name of the borehole	Section depth (meters)	Calculated pressure	Recorded pressure	Name of the borehole	Section depth (meters)	Calculated pressure	Recorded pressure
p-19	10-15	6.6623	5.14	TG-1	25-30	12.1123	11.61
p-19	15-20	7.2319	6.85	TG-1	30-35	12.2379	11.61
p-20	25-30	12.3819	10.15	TG-2	32-45	23.9081	23.22
p-22	15-20	9.9910	7.54				
p-23	50-53	24.0012	22				

Table 6 Values of relative error between calculated fracturing pressures and real pressures in percentages in water pressure test

Seymareh dam	Aghbolagh dam
4.75	2.6
4.8	5.22
3.93	22.43

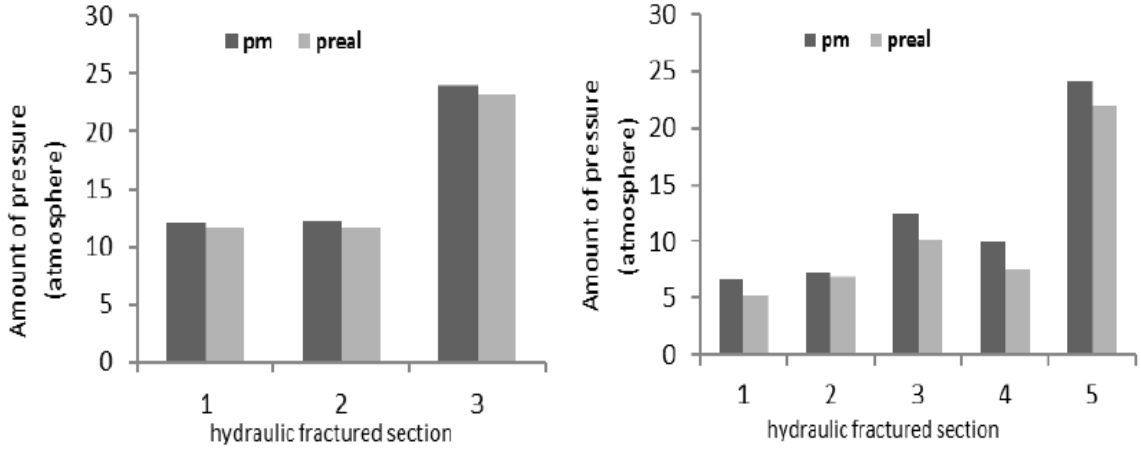

(a) (b)

Fig. 4 Convergence rate between measured fracturing pressure (P_m) and real fracturing pressure (P_{real}) in grouting operations in (a) Seymareh and (b) Aghbolagh dams

Table 7 Values of relative error between calculated fracturing pressures and real pressures in percentage in grouting operation

Seymarehdam	Aghbolaghdam
29.61	4.32
5.57	5.40
21.98	2.96
32.50	
9.09	

6. Comparison and validation of the results

In order to validate the modeling, relative error of the measured pressure (P_m) was compared to the real recorded pressure (P_{real}) obtained from the $E=((P_{real}-P_m)/P_{real})\times 100$. The results are shown in Tables 6 and 7.

According to the results shown in Figs. 3 and 4 and the values of relative error in Tables 6 and 7, it can be seen that there is a high degree of convergence and desirable correlation between the values of the real recorded pressure in Seymareh and Aghbolagh dam sites and the values measured through modeling in water pressure test and grouting. This shows that the proposed model has desirable precision in predicting and estimating the rate of hydraulic fracturing.

It can be seen, based on the overall results obtained by comparing the amounts of computational error in water pressure test and grouting operations, mathematical modeling in water pressure test is more accurate than grouting to calculate the necessary pressure for hydraulic fracturing. On average this error in water pressure test is 7.28 percent and in grouting operation is 13.92 percent.

The cause of these changes in the rate of error is due to differences in rheological properties of water and grout. Based on the assumptions used in the mathematical modeling for infiltrated fluid, it can be said, because the mathematical modeling is based on Newtonian fluid, and grout,

according to the water-cement ratio, from the Newtonian fluid will tend to Non-Newtonian fluid, correspondingly, modeling also faced with increasing computational error. As a result, calculation of the pressure in grouting operation by mathematical modeling will be more error than water pressure test.

7. Conclusions

What is studied in this study, Analysis fluid pressure rate that is infiltrated in water pressure test and grouting operations in order to prevent the phenomenon of hydraulic fracturing in rock mass. Because this phenomenon causes most of the joints to open, creates fractures in the rock mass and deteriorates its quality and also causes goals of grouting, namely sealing and improving the site not happen. Therefore, estimating the rate of grouting pressure which causes fractures is highly important. To do so, mathematical modeling and simulation of the joint conditions was conducted using a cylindrical shell and the pressure causing fracture was calculated. In order to validate the results, real values of hydraulic fracturing pressure recorded in water pressure test and grouting operations in Seymareh and Aghbolagh dams were used and the processes of change in real pressure values and calculated pressure values were controlled.

• The results showed that there is desirable convergence and correlation between these two sets of values.

• Calculation of the relative error between them showed that in water pressure test, the mathematical model in the sections of the Seymareh dam under study had the error values of 4.75, 3.93, 4.8 percent and in the Aghbolagh dam sections, the error values were equal to 22.43,5.22,2.6 percent.

• These results in grouting operation in Seymareh dam are equal to 9.09, 32.50, 21.98, 5.57 and 29.61 percent and in the Aghbolagh dam are 2.96, 5.40, and 4.32 percent.

• These data indicate that mathematical modeling can be used to predict the occurrence of hydraulic fracturing phenomenon in water pressure test and grouting operations and thus increase the efficiency and productivity of such processes.

• Based on the overall results, mathematical modeling in water pressure test is more accurate than grouting to calculate the necessary pressure for hydraulic fracturing.

• On average this error in water pressure test is 7.28 Percent and in grouting operation is 13.92 percent.

The cause of this changes is due to differences in rheological properties of water and grout. Because the mathematical modeling is based on Newtonian fluid, but grout is Non-Newtonian fluid and modeling faced with increasing computational error.

References

Arani, A.G., Kolahchi, R. and Barzoki, A.M. (2011), "Effect of material in-homogeneity on electro-thermo-mechanical behaviors of functionally graded piezoelectric rotating shaft", *Appl. Math Model.*, **35**(6), 2771-2789.

Arani, A.J. and Kolahchi, R. (2016), "Buckling analysis of embedded concrete columns armed with carbon nanotubes", *Comput. Concrete*, **17**(5), 567-578.

Broujerdian, V. and Kazemi, M.T. (2016), "Nonlinear finite element modeling of shear-critical reinforced concrete beams using a set of interactive constitutive laws", *J. Civ. Eng.*, **14**(8), 507-519.

Chang, M., Mao, T.W. and Huang, R.C. (2016), "A study on the improvements of geotechnical properties of in-situ soils by grouting", *Geomech. Eng.*, **10**(4), 527-546.
Cleary, M.P., Johnson, D.E., Kogsbøll, H.H., Owens, K.A., Perry, K.F., De Pater, C.J. and Mauro, T. (1993), "Field implementation of proppant slugs to avoid premature screen-out of hydraulic fractures with adequate proppant concentration", *Proceedings of the Low Permeability Reservoirs Symposium*, Denver, Colorado, U.S.A., April.
Creager, M. and Paris, P.C. (1997), "Elastic field equations for blunt cracks with reference to stress corrosion cracking", *J. Fract. Mech.*, **3**(4), 247-252.
Darn-Horng, H., Vu To-Anh, P. and Chi-Chang, H. (2016), "An experimental investigation on dynamic properties of various grouted sands", *Geomech. Eng.*, **10**(1), 77-94.
Economides, M.J. (1990), "Implications of cementing on well performance", *Dev. Petro. Sci.*, **28**, 1-1.
El Tani, M. (2012), "Grouting rock fractures with cement grout", *Rock Mech. Rock Eng.*, **45**(4), 547-561.
Fattah, M.Y., Al-Saidi, A.A. and Jaber, M.M. (2015), "Improvement of bearing capacity of footing on soft clay grouted with lime-silica fume mix", *Geomech. Eng.*, **8**(1), 113-132.
Fett, T. (1999), "Estimated stress intensity factors for semi-elliptical cracks in front of narrow circular notches", *Eng. Fract. Mech.*, **64**(3), 357-362.
Gang, Z., Xiaoshuang, Z., You, D. and Huayang, L. (2016), "Experimental study on the performance of compensation grouting in structured soil", *Geomech. Eng.*, **10**(3), 335-355.
Garagash, D.I. (2003), "Evolution of a plane-strain fracture driven by a power-law fluid", *Proceedings of the 16th ASCE Engineering Mechanics Conference*, Seattle, Washington, U.S.A., July.
Gulrajani, S.N., Nolte, K.G. and Romero, J. (1997), "Evaluation of the M-Site B-sand fracture experiments: The evolution of a pressure analysis methodology", *Proceedings of the SPE Annual Technical Conference and Exhibition*, San Antonio, Texas, U.S.A., October.
Houlsby, A.C. (1990), *Construction and Design of Cement Grouting: A Guide to Grouting in Rock Foundations*, John Wiley & Sons, New York, U.S.A.
Johnson, E. and Cleary, M.P. (1991), "Implications of recent laboratory experimental results for hydraulic fractures", *Proceedings of the Low Permeability Reservoirs Symposium*, Denver, Colorado, U.S.A., April.
Lhomme, T.P.Y. (2005), "Initiation of hydraulic fractures in natural sandstones", Delft University of Technology, The Netherlands.
Mack, M.G. and Elbel, J.L. (1994), "A Simulator for Modeling Acid Fracturing Treatments", *Proc.*
Rice, J.R. (1968), "Mathematical analysis in the mechanics of fracture", *Fract. Adv. Treat.*, **2**, 191-311.
Showkati, A., Maarefvand, P. and Hassani, H. (2015), "Theoretical determination of stress around a tensioned grouted anchor in rock", *Geomech. Eng.*, **8**(3), 441-460.
Shroff, A.V. and Shah, D.L. (1999), *Grouting Technology in Tunnelling and Dam Construction*, A.A. Balkema.
Tavakoli Mehrjardi, G. and Moghaddas Tafreshi, S.N. and Dawson, A. (2015), "Numerical analysis on Buried pipes protected by combination of geocell reinforcement and rubber-soil mixture", *J. Civ. Eng.*, **13**(2), 90-104.
Tolppanen, P. and Syrjänen, P. (2003), *Hard Rock Tunnel Grouting Practice in Finland, Sweden*, and *Norway-Literature Study*, Finnish Tunnelling Association.
Van Dam, D.B. (1999), "The influence of inelastic rock behaviouron hydraulic fracture geometry", Ph.D. Dissertation, Delft University of Technology, Delft, The Netherlands.
Van de Ketterij, R.G. (2001), "Optimisation of the near-wellbore geometry of hydraulic fractures propagating from cased perforated completions", Ph.D. Dissertation, Delft University of Technology, Delft, The Netherlands.
Vinegar, H.J., Wills, P.B., DeMartini, D.C., Shlyapobersky, J., Deeg, W.F.J., Adair, R.G., Woerpel, J.C., Fix, J.E. and Sorrells, G.G. (1992), "Active and passive seismic imaging of a hydraulic fracture in diatomite", *J. Petro. Tech.*, **44**(1), 28-90.
Wang, L. and Ni, Q. (2009), "A reappraisal of the computational modelling of carbon nanotubes conveying viscous fluid", *Mech. Res. Commun.*, **36**(7), 833-837.
Weijers, L. (1995), "The near-wellbore geometry of hydraulic fractures initiated from horizontal and

deviated wells", Ph.D. Dissertation, Delft University of Technology, Delft, The Netherlands.
Wong, H.Y. and Farmer, I.W. (1973), "Hydrofracture mechanisms in rock during pressure grouting", *Rock Mech*., **5**(1), 21-41.
Yew, C.H. and Weng, X. (2014), *Mechanics of Hydraulic Gracturing*, Gulf Professional Publishing.
Zhu, H.Y., Deng, J.G., Zhao, J., Zhao, H., Liu, H.L. and Wang, T., (2014), "Cementing failure of the casing-cement-rock interfaces during hydraulic fracturing", *Comput*. *Concrete*, **14**(1), 91-107.

CC